Applied Geochemistry 162 (2024) 105842

Contents lists available at ScienceDirect

Applied Geochemistry

journal homepage: www.elsevier.com/locate/apgeochem

Diffusion of HTO, ^{36}Cl and ^{22}Na in the Mesozoic rocks of northern Switzerland. II: Data interpretation in terms of an electrical double layer model

M.A. Glaus [a,*], L.R. Van Loon [a], R.A.J. Wüst [b,c]

[a] Paul Scherrer Institut, Forschungsstrasse 111, 5232, Villigen, PSI, Switzerland
[b] Nagra, Hardstrasse 73, 5430, Wettingen, Switzerland
[c] Earth and Environmental Science, James Cook University, 4811, Townsville, Australia

ARTICLE INFO

Editorial handling by: Adrian Bath

Keywords:
Surface diffusion
Anion exclusion
Electrical double layer
Mean potential
Heterogenous sedimentary rocks
Opalinus clay

ABSTRACT

It is widely recognised that diffusive transport of charged species in charged clay media must be consistently described for ions with different charge signs and numbers, as well as consistently with pore diffusion schemes for inert solutes that do not undergo interactions with the clay surface. This study presents a modelling approach that meets these requirements for the diffusion of tritiated water, $^{22}Na^{+}$ and $^{36}Cl^{-}$ tracer in heterogeneous Mesozoic sediment sequences of multiple deep-boreholes in northern Switzerland. The model uses an electrical double layer (EDL) approach and a discrete Donnan potential description of cation enrichment and concomitant anion depletion in the Donnan layer close to the basal (planar) clay surfaces to predict effective diffusion coefficients and capacity factors of the charged tracers. It incorporates diffusion data of tritiated water to determine the parameters related to the functional relationships between the accessible porosity and geometry factors with the total clay content as the main input variable. It also calculates concentration enrichment or depletion factors for mobile cationic and anionic species using relationships with the total clay content, such as the average density of surface sites or the thickness of the Donnan layer and the related volume fraction of free pore water. These factors are subsequently used to derive effective diffusion coefficients that include surface diffusion of cations and anion exclusion effects and the related capacity factors. Despite the various lithologies of the rock samples, where significant variability between carbonates and siliciclastic contents are observed, the model shows good agreement with experimental data. Discrepancies between experimental and modelled data are mainly due to inadequacies in the geometric description of diffusion pathways, rather than by potential bias in the calculation of concentration enhancement or depletion factors. However, the model approach assumes that diffusion in clay rock occurs via the pore space of clay minerals and treats all related parameters as simple average values, neglecting heterogeneity of mineral constituents and the unknown statistical distribution of the parameter values.

The model has identified the chemical composition of the equilibrium pore water as a significant influencing variable for prediction concentration enhancement or depletion factors and related effective diffusion coefficients. Experimental data obtained for different synthetic pore water compositions support this finding. The robustness of the model predictions across various types of lithologies and formations, all of which exhibit diffusion as the dominant transport mode, is crucial for the generic application of the EDL diffusion model to predict diffusion parameters for elements lacking experimental data.

1. Introduction

The assessment of the long-term safety of deep geological disposal of radioactive waste and spent fuel in clay-rich host rocks, like the Opalinus Clay and the adjacent, under- and overlying formations up to the next aquifer (the 'confining units') in Switzerland, requires a thorough

* Corresponding author. Paul Scherrer Institut, Laboratory for Waste Management, Forschungsstrasse 111, OHLD/002, CH-5232, Würenlingen und Villigen, Switzerland.
E-mail address: martin.glaus@psi.ch (M.A. Glaus).

https://doi.org/10.1016/j.apgeochem.2023.105842
Received 13 March 2023; Received in revised form 7 August 2023; Accepted 8 November 2023
Available online 22 November 2023

comprehension of the transport processes of solutes in porous media (both saturated and unsaturated) and the role related parameters (or best estimates) play. Since diffusion is the primary transport process in non-fractured geological formations, it is critical for estimating future radiation dose rates across rock intervals, aquifers or in the biosphere. Predictive calculations utilise deterministic simulations based on simplifying assumptions, such as effective diffusion coefficients representing the global diffusion of an element rather than its individual species (Nagra, 2014). Effective diffusion coefficients are scaling factors between the gradients of total element concentration in the aqueous phase and the diffusive fluxes of these elements according to Fick's first law. The effective diffusion coefficients of charged species in negatively charged argillaceous media are lump parameters that encompass (i) the bulk diffusion properties of the chemical species for the relevant state of the fluid with respect to viscosity and temperature, (ii) the geometric properties of the porous medium and (iii) the chemical enrichment of mobile species in the clay phase (cations) or depletion from the solution phase (anions) (Altmann et al., 2015; Maes et al., 2021; Shackelford and Daniel, 1991; Tinnacher et al., 2016).

As part of the Swiss deep geological radioactive waste repository site selection process, Nagra conducted deep borehole drillings to characterise the Mesozoic sedimentary units of northern Switzerland (Nagra, 2021). The first paper of this Virtual Special Issue (Mazurek et al., 2023) provides an overview of the drilling campaign locations and the characterisation of the lithologically diverse Malm/Jurassic/Triassic rock sequences. Abbreviations used in the context of these localities are given at the end of this contribution.

Diffusion measurements of various radiotracers on laboratory scale samples were conducted (Van Loon et al., 2023) to provide the experimental basis for the model development in the present contribution, and complementing earlier diffusion studies (e.g. Van Loon and Jakob (2005); Van Loon et al. (2003, 2004)). To investigate charge effects, the experimental study of Van Loon et al. (2023) included $^{36}Cl^-$ and $^{22}Na^+$ tracers and details of charged tracer modelling are presented here. The presence of permanent lattice charges near the basal (planar) clay surfaces leads to concentration enrichment of cationic species in the clay phase and a concurrent depletion of anionic species in the solution phase immediately adjacent to the clay surfaces relative to the respective concentrations in free water. Based on the assumption that some of the surface-associated cationic species are mobile, it is expected that the effective diffusion coefficients of $^{22}Na^+$ (normalised with the respective bulk diffusion coefficients) would be larger than those of HTO and the effective diffusion coefficients of $^{36}Cl^-$ smaller than those of HTO. The results generally confirmed these expectations (Van Loon et al. (2023).

The aim of this contribution is to evaluate the applicability of current models in describing the interaction of cationic and anionic species at planar clay surfaces using the entire data obtained from diffusion measurements (Van Loon et al., 2023). Previous studies, including van Schaik et al. (1966), Dufey and Laudelout (1975), Jensen and Radke (1988), or Molera and Eriksen (2002), have established that concentration gradients of mobile surface-associated species of cationic elements in negatively charged clays also contribute to overall observed fluxes. These gradients can explain the "unexpectedly large" effective diffusion coefficients of such elements because the definition of the effective diffusion coefficient relates the overall observed flux to the concentration gradients of the aqueous phase species, only. For compacted smectites, the concentration gradients of mobile surface-associated cationic species are even the dominant driving forces for diffusion (Glaus et al., 2007), which has been confirmed in diffusion experiments carried out under gradient conditions of the main electrolyte, in which gradients of the electro-potential act as an additional driving force (Glaus et al., 2013). Under such situations, the concentration gradients of mobile surface-associated cationic species were identified as the dominating driving force for diffusion. Similar findings were also made in the case of diffusion of transition metal cations in compacted illite (Glaus et al., 2015a). This latter study used an electrical double layer (EDL) approach for a quantitative description of the effective diffusion coefficients as a function of the properties of the clay surface and the solution composition. The present study focuses on the same EDL model (as shown in Fig. 1), which proposes that cationic surface species in the so-called Stern layer at planar clay surfaces are immobile, while species in the diffuse layer are mobile. The concentration ratios between the species in the diffuse layer and free pore water are determined, among other factors, by the (mean) Donnan potential resulting from the excess free negative surface charges. The overall charge neutralisation is achieved by the balance between the sum of charges of all cations and anions present in the EDL and the sum of permanent negative lattice charges.

The model used in this study (Fig. 1) assumes that ions in free water (blue charge signs) and the ion swarm in the Donnan layer (green charge signs) are mobile, while cationic species in the Stern layer (red charge signs) are immobile surface complexes. The blue domain (Fig. 1) represents free water with bulk properties where charge neutralisation is fulfilled by solution anions and cations. The green domain represents the Donnan layer, a charged solution phase exhibiting the opposite net charge of the clay surface. The local concentration gradients parallel to the clay surface in the different domains result in individual flux contributions (J_i) if there is a concentration difference of a tracer cation species. This model has been applied successfully to determine diffusion and retardation properties of a wide range of chemically different elements in compacted illite (Glaus et al., 2015a, 2020) and Opalinus Clay (Appelo et al., 2010). The term 'Donnan layer' is considered as a special case of the more general term 'diffuse layer', where the potential curve is not explicitly defined (mostly assumed as exponential according to the Poisson-Boltzmann equation), while in the former, it is defined as a homogeneous discrete step function.

The main scientific question addressed in this research is whether the EDL model for illite, which was validated to be transferable to Opalinus Clay by Glaus et al. (2021) using a $^{57}Co^{2+}$ tracer, is transferable to sedimentary rocks with variable mineralogies of clays, carbonates and other silicates. The EDL model comprises parameters that cannot be directly measured or which may differ in a specific manner for the rock samples from different lithologies, such as the average pore diameter or the thickness of the Donnan (or EDL) layer (d_{DL}) at the surfaces of a clay pore. Another objective of this study is to assess whether generic average parameter values can adequately describe the experimental results. The predictions of the model primarily involve the effective diffusion coefficient (D_e, [m^2 s^{-1}]) and the rock capacity factor (α, [–]), which are related to the apparent diffusion coefficient (D_a) by eq. (1)

$$D_e = D_a \cdot \alpha \tag{1}$$

The rock capacity factor, α, can further be expanded according to eq. (2) which allows for secondary information to be derived from α related to the diffusion behaviour and to the distribution of a diffusing species between the aqueous and the clay phase.

$$\alpha = \varepsilon + R_d \rho_b \tag{2}$$

ε [–] is the accessible porosity, R_d [m^3 kg^{-1}] the sorption distribution coefficient and ρ_b [kg m^{-3}] the bulk-dry density. For non-sorbing species ($R_d = 0$), like neutral and many anionic species, α equals ε. In the case of

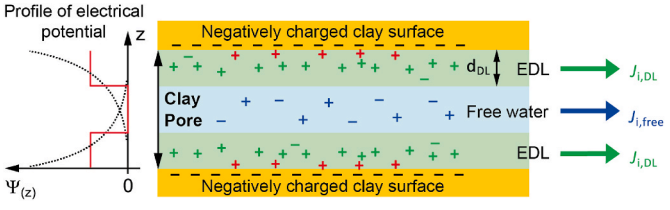

Fig. 1. Schematic representation of the Donnan approach for an electrical double layer (EDL) for a planar pore geometry. Details on the symbols and colours are given in the main text. (Sketch adapted from Maes et al. (2021)).

uncharged tracers like HTO, it is normally assumed that ε equals the total porosity. In the case of anionic species, ε may be represented by the 'anion-accessible' porosity (ε_{An}) for the assumption of exclusion of anions from parts of the total porosity. 'Anion exclusion' is different from the situation shown in Fig. 1, where anions are present in both the diffuse layer and the free porosity. A more detailed discussion of anion exclusion effects and their formal treatment in an EDL model can be found in section 2.4 of the present work and in Zwahlen et al. (2023).

As a pure modelling study, this contribution is closely related to the two companion papers of Part I by Van Loon et al. (2023), which provides the entire basic set of experimental data, the technical details related to the diffusion measurements and the modelling methods to describe the 'geometric effects', and Part III by Van Laer et al. (2023) which presents a benchmark study of diffusion measurement and modelling approaches carried out at PSI and at SCK-CEN (Belgium) using a selection of five rock samples from the complete series of diffusion samples examined.

2. Model definitions and parametrisation

The EDL model (cf Fig. 1) is an extension of the classic cation exchange model for the uptake of cations at the planar clay surfaces. There, the negative charges near the planar clay surfaces are completely neutralised by charge compensating cations (Baeyens and Bradbury, 2004; Stumm and Morgan, 1996). The EDL extension assumes that only a fraction of the planar clay charges is directly compensated by cations at the surface (Stern layer), leaving a number of free charges that give rise to electrostatic effects (Appelo et al., 2010). These free charges are counterbalanced by loosely bound cations which are assumed to be mobile, while those in the Stern layer are treated as immobile (Glaus et al., 2020). The Stern layer species are thermodynamically treated as surface complexes, the stability of which is given by a surface complexation constant and an additional surface potential term (Appelo and Postma, 2005).

The EDL model using a constant Donnan potential in a given volume near the surface (the Donnan layer) has been successfully applied to describe the effects of enhanced diffusion rates of cationic species in charged clays (Glaus et al., 2015a, 2020). D_e is calculated from the superposition of parallel diffusive fluxes in the free pore water and in the Donnan layer as

$$D_e = \frac{\varepsilon}{G} D_w \left(f_{free} + f_{DL} \frac{c_{DL}}{c} q_\eta \right) \tag{3}$$

The ratio c_{DL}/c represents the concentration ratio of charged species between the Donnan layer and the free aqueous phase. ε is the total porosity, G [–] the geometry factor, f_{free} [–] the volume fraction of free pore water, f_{DL} [–] the volume fraction of the Donnan layer, D_w [$m^2\ s^{-1}$] the diffusion coefficient in bulk water and q_η [–] the ratio of viscosity of free and EDL water. Note that the application of eq. (3) is restricted to a series of prerequisites, such as a fast equilibration of the thermodynamic equilibrium between Donnan layer and free water species compared to the dynamics of diffusion, or the condition of linear sorption. For the present application of eq. (3) to the diffusion data of the charged radioisotopes, it is assumed for simplicity that G has the same value as measured for HTO, both in the free aqueous pore phase and in the Donnan layer, and that q_η equals 1. For uncharged species, such as HTO, the concentration ratio c_{DL}/c equals 1 and eq. (3) is reduced to

$$D_e = \frac{\varepsilon}{G} D_w \tag{4}$$

because $f_{free} + f_{DL} = 1$.

With fixed assumptions for G and q_η as described, D_e values depend on all parameters that may affect f_{free}, f_{DL} and the concentration ratio c_{DL}/c. The latter expression is calculated for all charged species from an electrical potential term assuming equal activity coefficients for species in the free aqueous phase and in the Donnan layer (cf. eq. (5))

$$\frac{c_{DL}}{c} = \exp\left(\frac{-zF\Psi_D}{RT} \right) \tag{5}$$

z is the charge number, F the Faraday constant (96,485 C mol^{-1}), R the universal gas constant (8.314 J K^{-1} mol^{-1}), T the temperature (K) and Ψ_D the (mean) Donnan potential. Ψ_D is obtained by iteratively solving the defining equations comprising (i) the overall charge neutrality for solution and solid and (ii) eq. (5) for all charged species present in the system (Appelo et al., 2010). According to the conventions regarding the signs of charge numbers and the involved potential, cationic species are enriched in the Donnan layer compared to their concentrations in the bulk aqueous phase ($c_{DL}/c > 1$) while anionic species are depleted ($c_{DL}/c < 1$). For the present application of the EDL diffusion model, the parameters affecting f_{free}, f_{DL} and the concentration ratio c_{DL}/c can be grouped into different categories. This compilation also provides the derivation of the parameters for the purpose of application to clay rock and the values chosen as default settings.

2.1. Geometric properties of the pore space

Here, the assumption of infinitely long planar pores, restricted to clay domains only, is taken. The pore width (d_P [m]) for a planar pore with much longer lateral dimensions compared to thickness is approximately proportional to the ratio of pore surface area (A_p [m^2]) and pore volume (V_p [m^3]) and thus to the specific surface area (A_{sp} [$m^2\ kg^{-1}$]) and the solid:liquid ratio (ρ_{SL} [$kg\ m^{-3}$]), according to:

$$d_p = \frac{2V_p}{A_p} = \frac{2}{A_{sp}\rho_{SL} f_c} \tag{6}$$

Note that ρ_{SL} is related to the mass of clay rock per pore volume. The restriction that porosity is present only in clay minerals is realised in eq. (6) by the introduction of the clay mass fraction (f_c), defined as the mass ratio between clay and rock. The Donnan thickness (d_{DL} [m]) is assumed to be a multiple (n_{DL}) of the Debye length ($1/\kappa$, which is, among other factors, a primary function of the ionic strength, cf. Appelo and Postma (2005)). Thus:

$$d_{DL} = \frac{n_{DL}}{\kappa} \tag{7}$$

A commonly used default value for n_{DL} is 2, as established in previous research (Glaus et al., 2015a). Based on the simplified illustration in Fig. 1, it is assumed that there are no domains where complete anion-exclusion exist, even though such areas have been identified in dense clay media (Chagneau et al., 2015; Wigger et al., 2018). Therefore, the volume fraction of free pore water f_{free} can be calculated as follows (note that there are two Donnan layers on each side of a planar pore)

$$f_{DL} = \frac{2d_{DL}}{d_p} \text{ and } f_{free} = 1 - f_{DL} \tag{8}$$

For the implementation of the model in Phreeqc (Appelo and Wersin, 2007), it is important to prevent situations where $2d_{DL} > d_p$, as this can result in negative values of f_{free}. To address this issue for such conditions, f_{free} is limited arbitrarily to 0.01 and d_{DL} to $0.99 d_p/2$.

The geometric properties of the rock samples are derived from the same empiric relationships of ε and G on the clay content (W_c, $W_c = f_c$ x100%) as described the companion paper Van Loon et al. (2023).

$$\varepsilon = m_1 \left(1 - e^{-m_2 \cdot W_c} \right) \tag{9}$$

$$G = a_1 + e^{a_2 \cdot W_c} \tag{10}$$

The empiric parameters m_1, m_2, a_1 and a_2 were evaluated in Van Loon et al. (2023) from fitting the diffusion data of HTO to eqs. (9) and (10). The validity of the model could be directly assessed by comparing the D_e values measured for HTO with the modelled values according to eq. (4).

The numeric values of the best estimates are $m_1 = 0.1444 \pm 0.0063$, $m_2 = 0.0398 \pm 0.0045$, $a_1 = 10 \pm 2$ and $a_2 = 0.0515 \pm 0.0016$. The specified parameter uncertainties are at the 1σ confidence level. These parameter values are also used for the present purpose of calculating the accessible porosity and geometry values in the simulation of the D_e values of the $^{36}Cl^-$ and $^{22}Na^+$ tracers (cf. eq. (3)). The reasons for using eqs. (9) and (10) for the calculation of the geometric properties of the rock samples instead of Archie's relationship (e.g. Van Loon and Mibus, 2015) are explained in detail in Van Loon et al. (2023).

The bulk-dry density (ρ_b [kg m^{-3}]) and ρ_{SL} were calculated, assuming an average grain (or material) density (ρ_s [kg m^{-3}]) of the solid rock of 2700 [kg m^{-3}], which was chosen as an approximate average from all rock samples obtained from the deep drilling campaign (cf. Fig. A1 of the Appendix). Both quantities depend thus on W_c according to the dependence of ε on W_c (cf. eq. (9)

$$\rho_b = \rho_s(1-\varepsilon) \text{and } \rho_{SL} = \frac{\rho_b}{\varepsilon} \quad (11)$$

A_{sp} is set to 10^5 [m^2 kg^{-1} of clay], a typical value for illite, which is for simplicity assumed to be the representative clay mineral in the rock samples. Alternatively, it would also be possible to use a representative value (~6×10^4 [m^2 kg^{-1} of clay]) of all samples of the drilling campaign used for the purpose of diffusion measurements (cf. Fig. A2 of the Appendix). This choice is somehow irrelevant because it cannot be resolved from the selection of the assumptions regarding n_{DL}.

2.2. Mineralogic properties of the solid

The mean value of cation exchange capacity (CEC [mol kg^{-1} of clay]) measurements, obtained using both the Ni-ethylenediamine and the Cs isotope dilution methods on the rock samples collected during the deep drilling campaign, has been extrapolated to 100% clay (CEC_{100}). The estimated value of CEC_{100} is approximately ~0.21 mol kg^{-1} of clay (as shown in Fig A3 of the Appendix). In order to facilitate the practical implementation in Phreeqc, the CEC is converted to a volumetric basis (CEC_{vol}) using eq. (12), which expresses CEC as moles of cations per volume of pore water:

$$CEC_{vol} = CEC_{100} \cdot f_c \cdot \rho_{SL} \quad (12)$$

2.3. Chemical properties of the solution and the clay surfaces

Van Loon et al. (2023) employed four different compositions of synthetic pore water (SPW) to conduct the diffusion measurements. Their compositions (Table 1) were derived from the results of advective displacement studies of selected laboratory-scale samples in order to provide a maximum of representativity for the adjacent layers. The abbreviations in their acronyms correspond to the names of the locations of the drilling sites.

The primary aim of using SPWs was to prevent concentration gradients with regards to electrolyte concentrations between the pore solutions of the rock samples and the electrolyte solutions in contact with these during the phase of tracer through-diffusion measurements. To attain such conditions, the rock samples were pre-equilibrated with the SPWs for sufficient periods before adding the tracer.

Table 2, as reported by Glaus et al. (2021), provides the surface complexation constants for the Stern layer species. These constants serve as the primary variables that determine the negative excess surface charge and, consequently, the species distribution between the free aqueous phase and the Donnan layer.

2.4. Calculation of diffusion and sorption/depletion parameters using the EDL model

For the simulations of D_e (cf. eq. (3)) values, the element-specific D_w values are taken from the literature (Li and Gregory, 1974), while the total porosity (ε) and geometry factor (G) are derived as discussed above from empiric relationships with W_c (cf. eqs. (9) and (10)) and the parameter values specified in the respective text. The base thermodynamic equilibrium data were obtained from the PSI Nagra 2020 thermodynamic database (Hummel and Thoenen, 2023). A summary of all parameters, constants and variables used for the EDL simulations is provided in Table A1 of the Appendix.

The parameter predictions of the EDL model are not only restricted to D_e values which are derived from the quasi-steady-state flux behaviour in a through-diffusion experiment (Glaus et al., 2015b). The retardation behaviour is characterised by the rock capacity factor α (cf. eq. (1)) which is related to the R_d value according to eq. (2). The simulation of R_d values for cationic species through the use of the EDL model is based on the definition of R_d as the ratio of the total number of species bound to the clay divided by the total number of species present in solution, normalised for the mass of the clay and volume of the solution. The bracket expression in eq. (3) cannot be directly applied for the calculation of R_d, because the c_{DL}/c ratio only represents the equilibrium conditions of the Donnan layer species. To accurately calculate R_d, the contribution of the Stern layer species must also be considered and included in the calculation. All of these characteristics can be obtained directly from the output data of Phreeqc. The calculation of R_d values according to eq. (2) for cationic tracers like $^{22}Na^+$ further involves the assumption that the accessible porosity of these species equals the accessible porosity of HTO.

Eq. (2) is formally also applied within the scope of an anion-exclusion model, in which a fraction of the pore volume is assumed to be completely devoid of anions. The anion exclusion volume is not identical to the Donnan volume because anions distribute both to free pore water and Donnan volume in the EDL model (cf. Fig. (1)). Nevertheless, the results obtained from the EDL model can be readily converted to an anion exclusion model. With regards to eq. (3), the conversion is done ($q_\eta = 1$) by

Table 1
Composition of the synthetic pore water (SPW) used in the diffusion experiments.

Element	Concentration (M)			
Name	SPW-BOZ	SPW-BUL	SPW-STA	SPW-TRU
Na	1.40×10^{-1}	3.43×10^{-1}	1.56×10^{-1}	2.44×10^{-1}
K	7.76×10^{-4}	1.91×10^{-3}	1.91×10^{-3}	1.64×10^{-3}
Ca	9.24×10^{-3}	3.83×10^{-2}	3.50×10^{-2}	2.22×10^{-2}
Mg	3.94×10^{-3}	1.76×10^{-2}	1.76×10^{-2}	1.56×10^{-2}
Sr	1.15×10^{-4}	3.33×10^{-4}	3.33×10^{-4}	2.89×10^{-4}
Cl	8.28×10^{-2}	4.02×10^{-1}	2.19×10^{-1}	2.72×10^{-1}
S (as SO_4)	4.21×10^{-2}	2.75×10^{-2}	2.22×10^{-2}	2.43×10^{-2}
C (as HCO_3)	7.05×10^{-4}	4.13×10^{-4}	4.13×10^{-4}	4.87×10^{-4}
pH	7.90	7.56	7.56	7.68
I	0.190	0.505	0.306	0.354

Table 2
Surface complexation constants for the formation of dominant Stern layer species. The constant for H^+ has been omitted because such complexes are hardly formed at the pH of the experiments. The constant for Sr^{2+} has been adjusted to that of Ca^{2+}.

Site types	$\log^{Su}K$
Na^+	−0.7 [a]
K^+	−1.0 [b]
Ca^{2+}	0.104 [b]
Mg^{2+}	0.107 [b]

[a] Taken from Appelo and Wersin (2007) and references cited therein.
[b] Adapted values which produce a similar cation loading as a pure cation exchange model (Glaus et al., 2021).

$$\alpha = \varepsilon_{AN} = f_{free} + f_{DL}\frac{c_{DL}}{c} \quad (13)$$

This conversion allows for comparison of the present model to different conceptual approaches to predict Cl-accessible porosity fractions assuming full anion exclusion (Zwahlen et al., 2023). Using the accessible porosity data of the $^{36}Cl^-$ tracer derived from the EDL model, the respective anion-accessible porosity fractions (f_{AN}) were calculated according to eq. (14), where ε_{HTO} denotes the accessible porosity of HTO.

$$f_{AN} = \frac{\varepsilon_{AN}}{\varepsilon_{HTO}} \quad (14)$$

3. Results and discussion

In the study conducted by Van Loon et al. (2023), it was found that the composition of the pore water has a significant impact on the diffusion parameters of $^{36}Cl^-$ and $^{22}Na^+$ tracers. The authors concluded that, for a given type of lithology, the pore water composition has a greater influence on these parameters than the location or area from where the samples were taken throughout the study areas. Consequently, it is considered a practical approach to model the entire set of diffusion using generic parameters for pore geometry and clay properties, while accounting for the specific composition of the pore water.

As shown in section 2.1, the dependence of the pore geometry on the clay content has a pivotal impact on the equilibrium distribution of charged species between the free aqueous phase and the Donnan layer. Fig. 2 shows the spatial extension of the Donnan thickness in comparison to the pore width. The particular dependence of these two quantities on the total clay content is governed by the assumption that the porosity of the clay rock is limited to the domains containing the clay mineral (cf. eq. (6)). This is clearly a gross simplification of reality which is made here for the purpose of reducing the model description to a minimum of adjustable parameters. According to eq. (9), the limiting total porosity would tend towards zero for a zero total clay content. This is certainly outside the scope of reality and for this reason, the model cannot be indiscriminately to such cases. Accordingly, the model curves in Fig. 2 and the subsequent diagrams are interrupted arbitrarily at very low total clay contents. As can be seen from Fig. 2, the pore diameter decreases with increasing total clay content. This trend is in agreement with the hypothesis expressed in Mazurek et al. (2023) and Van Loon et al. (2023) that the clay compaction increases with increasing clay content. The Donnan thickness is further governed by the pore water properties, viz. The ionic strength of the pore water. In order to avoid situations of overlapping double layers, the limitation of $2d_{DL} > d_p$ has been introduced (cf. section 2.1). At the transition point, at which this condition is reached, the Donnan thickness is truncated to $0.99d_p/2$. These situations are represented in Fig. 2, where the black curves reach the blue line.

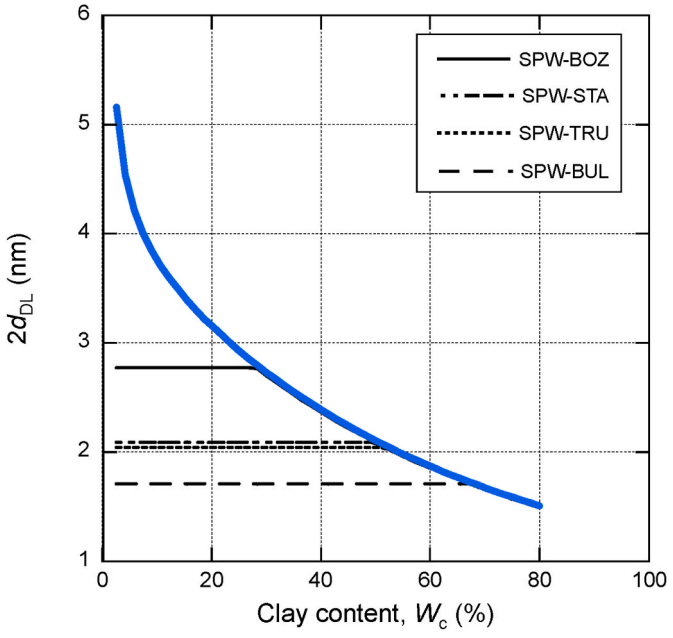

Fig. 2. Twice Donnan thickness ($2d_{DL}$) as a function of clay content calculated for the various SPW's using the default model settings (black lines). The blue line represents the pore width (d_p). The points, at which the black lines reach the blue line indicate that d_{DL} has been truncated to $0.99d_p/2$ according to the condition $2d_{DL} > d_p$ (cf. section 2.1).

Figs. 3–5 provide a visual comparison between the model predictions (lines) for $^{36}Cl^-$ and $^{22}Na^+$ (including those of HTO for completeness) and the experimental data grouped into selected different lithologies. The plots are arranged based on the different pore water compositions used in the experiments starting with the lowest ionic strength (in JO) (Fig. 3) to the highest ionic strength (in NL) (Fig. 5). The model curves are calculated according to the information given in section 2.

The data from Marthalen-1 and Trüllikon-1 (ZNO area), and Stadel-2/-3 (NL area), which used similar pore water compositions, are shown together in a single plot (Fig. 4). Lithologies are categorised as claystone, argillaceous sand/siltstones (arg sst/slt) and limestone rock types. The clay-rich Opalinus Clay (OPA) is represented by a lighter variant of violet (Figs. 3, 4 and 5). No experimental uncertainties are shown in these plots for clarity reasons. The uncertainties on the best-fit parameter values were evaluated in the course of the Matlab parameter optimisation routine on a 95% confidence level (Van Loon et al., 2023). On a relative scale, the uncertainties are less than 10% for the effective diffusion coefficients D_e of most tracers. The calculated relative uncertainties on the α values (accessible porosities) of HTO are in the order of less than 10 %, while these are significantly larger in the case of $^{36}Cl^-$ (average of ~40%, single cases up to almost 100%). The calculated uncertainties on the R_d values of $^{22}Na^+$ are of the order of 10–15%. Any measurement data that deviate significantly from the model are marked for discussion by their sample identity (drilling depth). Note that the α values for HTO represent the diffusion-accessible porosity which is commonly assumed to be identical with the total porosity.

In terms of providing an overall description of the average system behaviour, the model predictions demonstrate a satisfactory agreement with the experimental data, although certain biases are observed in various aspects. This reaffirms the suitability of the fundamental data for illite to be applied to Opalinus Clay, as previously established in earlier research (Glaus et al., 2021). The choice of the model parameters does not need to be adjusted specifically for the rock samples investigated. The model can also be applied to a broad range of other formations and lithologies within the Mesozoic sedimentary rocks where diffusion transport dominates. There, it is even valuable at low clay contents. This is unexpected as the model only considers clay mineral properties and does not take into account other mineral constituents like carbonates or other silicates. However, as demonstrated by Van Loon et al. (2023), the diffusion data (D_e values) of the clay- and quartz-rich rock samples exhibit smaller variability than those of the carbonate-rich samples. This is also evident in Fig. 4, that shows the diffusion data from the boreholes of Marthalen and Stadel, where the focus of the sample analysis was on the over- and underlying geological units rather than the Opalinus Clay formation.

Figs. 3–5 demonstrate the impact of surface diffusion, which is active in the case of $^{22}Na^+$. This is seen by comparing the model curves for $^{22}Na^+$ and HTO. The effect decreases as ionic strength increases. It should be noted that the bulk diffusion coefficient of HTO is larger (2.2×10^{-9} m^2 s^{-1}) than that of $^{22}Na^+$ (1.3×10^{-9} m^2 s^{-1}). To show an unbiased effect of surface diffusion, the model curves should be normalised by the ratio of these bulk diffusion coefficients. The reason for increased model discrepancies in some experimental data is due to intrinsic inconsistencies of the underlying diffusion measurements. This is the case in the marked $^{22}Na^+$ cases shown in Figs. 3, 4 and 5 by

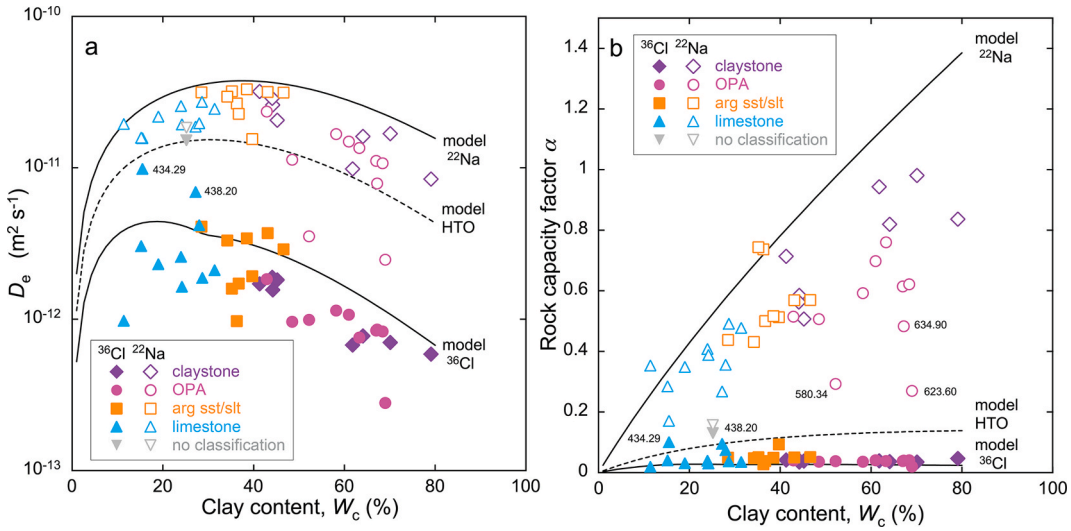

Fig. 3. Comparison between experimental data and the EDL simulations involving samples from the JO study area (Bözberg-1/-2) using SPW-BOZ. Note that α equals the anion-accessible porosity for the $^{36}Cl^-$ tracer (eq. (13)); R_d values can be derived from α in the case of $^{22}Na^+$ tracer according to eq. (2).

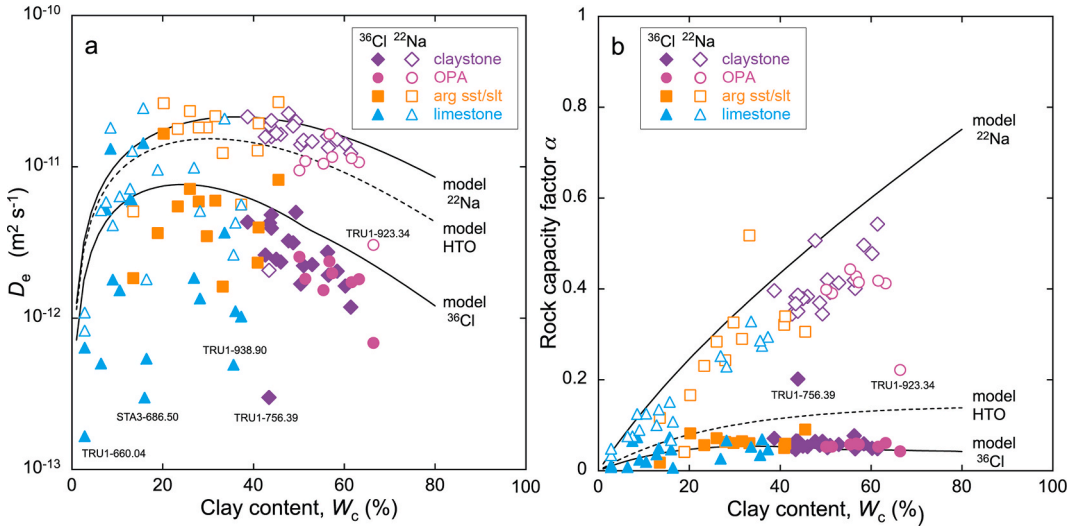

Fig. 4. Comparison between experimental data and the EDL simulations involving samples from NL (Stadel-2/-3) and ZNO (Trüllikon-1, Marthalen-1) using SPW-STA and SPW-TRU, respectively. No systematic differences could be found for the diffusion behaviour of samples of the different study areas. Note that α equals the anion-accessible porosity for the $^{36}Cl^-$ tracer (eq. (13)); R_d values can be derived from α in the case of $^{22}Na^+$ tracer according to eq. (2).

specification of the drilling depth. In some of those cases, a significant mass discrepancy between the tracer depletion in the source reservoir and the mass transferred to the target reservoir and clay was noted. The reason for this issue could not be resolved.

As expected, the diffusion data of $^{36}Cl^-$ exhibits the opposite trend, showing an increasing alignment to the D_e values of HTO with increasing ionic strength. The $^{36}Cl^-$ results marked by depth in Fig. 3 are not due to experimental inconsistencies, but rather to samples with a high content of goethite. This raises a broader discussion of the α values for anions, which are commonly assumed to be non-sorbing species and that the observed α values for anions are representative of the anion-accessible porosity. However, it has been established that anions may significantly sorb on clay minerals, in particular on kaolinite and, to a lesser extent, on illite (Chen et al., 2018). Although the underlying mechanism is not fully understood, anions may sorb via electrostatic forces on protonated aluminol sites, which are abundant on the oxidic surfaces of kaolinite. Sorption of anions increases as the pH decreases. As the result, the α values will be higher than the anion-accessible porosity in such cases. A high content of goethite (or other iron oxides) in clay rock samples would particularly enhance anion sorption.

The elevated discrepancies between experimental data and model prediction for other cases of $^{36}Cl^-$ results in Figs. 4 and 5 are not due to obvious experimental inconsistencies or distinct differences in rock properties. The geometric factors are notably high in some carbonate-rich rock samples, in particular those with high organic carbon content. However, no generic correlation can be found between the organic content and the geometric factors for HTO (cf. Fig. A4 of the Appendix).

In some cases (Figs. 3a, 4a and 5a), the experimental diffusion coefficients of $^{36}Cl^-$ exhibits more significant outliers than those of $^{22}Na^+$. The significance of this difference may be evaluated using statistical methods, such as the chi-square analysis. However, a quantitative statistical analysis of the data deviations from the model curve may not be informative given the nature of the model curves representing near-blind predictions instead of error-minimised best-fits. Additionally, the logarithmic scale of the representation of the D_e values in Fig. 3a, 4a and 5a may be misleading as negative errors can appear larger than positive ones. To avoid bias, Fig. 6a shows a representation of the relative residuals (eq. (15)) on absolute, rather than logarithmic scale.

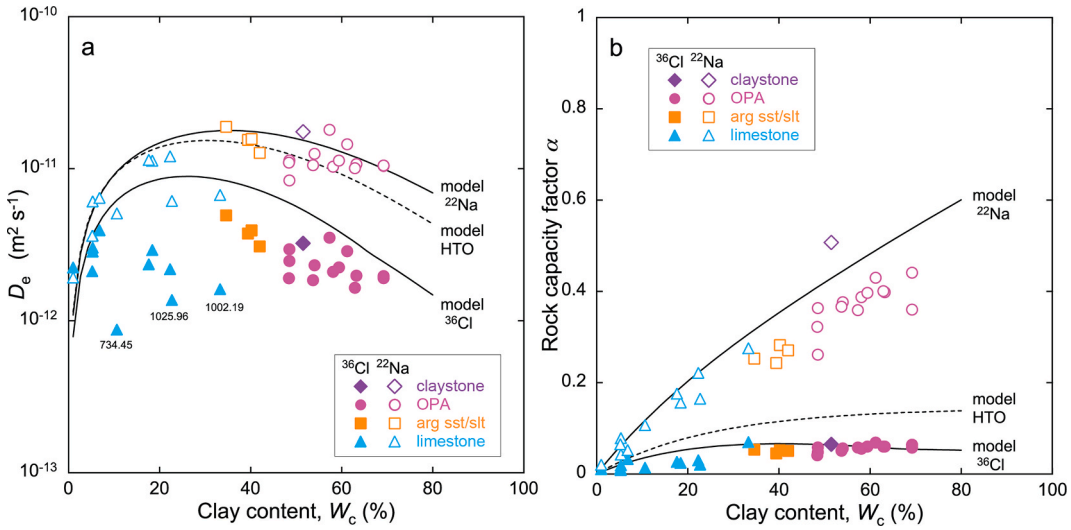

Fig. 5. Comparison between experimental data and the EDL simulations involving samples from NL (samples only from Bülach-1) using SPW-BUL. Note that α equals the anion-accessible porosity for the $^{36}Cl^-$ tracer (eq. (13)); R_d values can be derived from α in the case of $^{22}Na^+$ tracer according to eq. (2).

$$\Delta_r y = \frac{y_{exp} - y_{mod}}{y_{mod}} \quad (15)$$

$\Delta_r y$ represents in the present case the relative residuals of D_e values with subscript exp denoting the experimental values and mod the model values. A $\Delta_r y$ of 1 denotes thus a deviation of 100%. Fig. 6a indicates that the deviations from the model are approximately similar for all tracers, with a tendency towards lower deviations for clay contents exceeding ~50%. Fig. 6b shows the relationship between the relative residuals of D_e values of the charged tracers as a function of the relative residuals of HTO, revealing correlated data sets with similar slopes. This finding suggests that bracket expression inadequacies in eq. (3) are not the primary reason of the model discrepancies. The assumption of an average pore width, which may be biased, and the generalization that porosity is only linked to clay minerals may contribute to these inadequacies. Zwahlen et al., 2023 provide a more detailed discussion of this topic.

Fig. 7 shows the dependence of the bracket expression of eq. (3) on the 'concentration enhancement/depletion factor', as a function of pore width, which is calculated using simple average values based on eq. (6). If non-clay minerals make up a significant portion of the porosity, this equation may not be suitable to adequately evaluating concentration enhancement/depletion effects. Despite the opposite behaviour of the model curves of the $^{36}Cl^-$ and $^{22}Na^+$ tracers, Fig. 6b shows an almost direct correlation. Consequently, for the majority of the data, it can be concluded that the geometric effects rather than the 'chemical contributions' are the main reasons for the deviations between experimental data and model curves. Also note that the behaviour of positively and negatively charged species in Fig. 6b is not precisely symmetrical. Nevertheless, these nuances are lost by the typical data uncertainties and the minor role of the electrostatic factors to the overall uncertainties.

The sole systematic deviation in the model is an overestimation of the capacity factors for the $^{22}Na^+$ data. This can be attributed to an overestimation of the occupancy of the planar clay surfaces with Na^+ by the thermodynamic data shown in Table 2, which was derived from illite data. The formal cation selectivities, obtained by summing the amounts of cationic species present in the Stern layer species and those in the Donnan layer, are not in full agreement with the data shown in Table 2. However, generic values are still used for the modelling and in view of the tolerable model discrepancies, no further adjustment of those thermodynamic base data is made.

An important parameter in evaluating palaeogeological stable-isotope concentration profiles (Aschwanden et al., 2023; Wersin et al., 2023) is the porosity fraction accessible for different anions, which is shown for $^{36}Cl^-$ in Fig. 8 along with experimental uncertainties for all study sites. The data are calculated according to eqs. (13) and (14). The propagated experimental uncertainties are quite large and in many cases

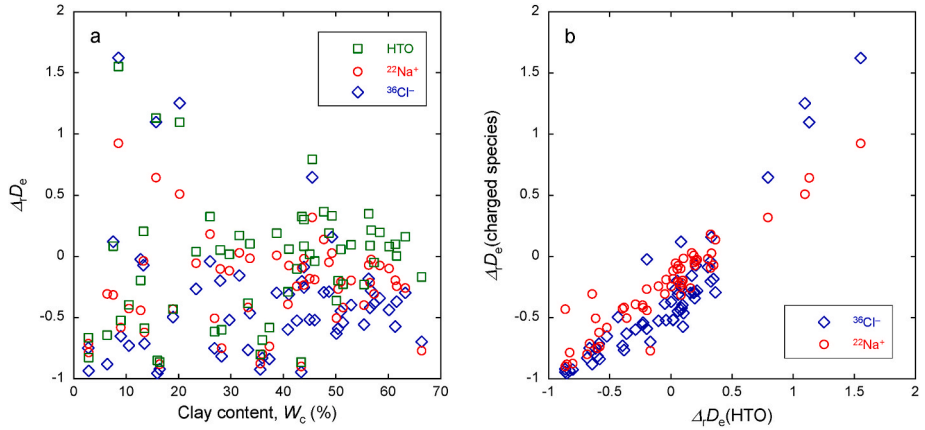

Fig. 6. Representation of relative residuals (eq. (15)) of effective diffusion D_e values shown in Fig. 4a (left-hand plot) and correlation between the relative residuals of charged species as a function of the relative residuals for HTO (right-hand plot).

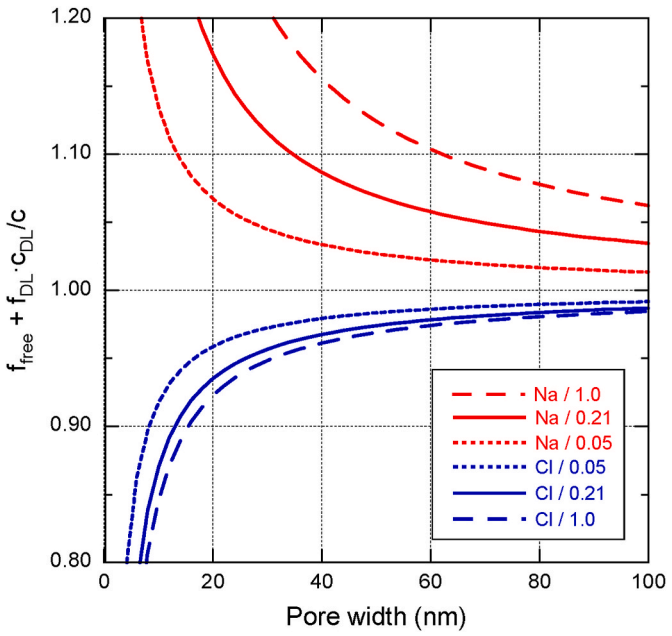

Fig. 7. Enhancement/depletion factors (bracket expression in eq. (3)) for Na^+ and Cl^- as a function of pore width. The values after the slash denotes the number of sites (mol kg^{-1}). In agreement with the simulations shown in Fig's. 3–5, q_η is assumed to take a value of 1.

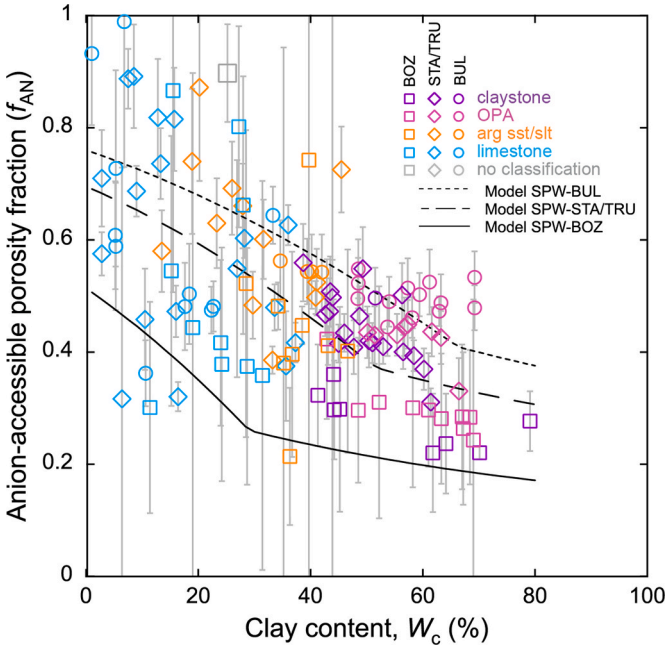

Fig. 8. Anion-accessible porosity fraction for $^{36}Cl^-$ versus clay fraction showing the data of all study areas and different SPWs composition models. The data related to SPW-BUL are shown as circles, those related to SPW-STA and SPW-TRU as diamonds, and those to SPW-BOZ as squares.

due to the high experimental uncertainties related to the anion-accessible porosity for $^{36}Cl^-$. The effect of pore water composition on f_{AN} is clearly visible in the clay-rich rock samples, which have less experimental uncertainty and are very well represented by the model curves. The distinction becomes less noticeable in samples with low clay contents, however, most of the data agree with the model predictions despite the large uncertainties generally involved. Fig. 8 highlights that the model assumptions taken in the simulations of palaeogeological isotope profiles of charged species must take into account the composition of the in situ pore waters, such as the ionic strength.

Zwahlen et al., 2023 present an empirical model that relates Cl-accessible porosity fraction derived from various approaches to clay fraction. At clay contents >30 %, the modelled accessibilities are close to constant at approximately 0.32 for samples from the JO area (BOZ) and at 0.47 in case of ZNO and NL. This difference is attributed to the significantly lower ionic strength of the in situ porewater of JO compared to the two other regions.

4. Conclusions

Based on a comprehensive dataset of diffusion data from the Mesozoic sedimentary rocks in northern Switzerland, the EDL model's prediction for $^{22}Na^+$ and $^{36}Cl^-$ show remarkable consistency with the experimental diffusion data. The settings for the model were previously used for illite systems and found to be transferable to Opalinus Clay (i.e. using similar values for the parameter settings in terms of CEC and specific surface area) (Glaus et al., 2021). The settings are applicable also for other types of argillaceous rocks in which illite is not exclusively the dominating clay mineral. The robustness of the model predictions for these different types of lithologies and formations, all of which shows diffusion as the dominant transport mode, is very important for a generic application of the EDL diffusion model to predict diffusion parameters for elements for which no experimental data exist. Despite a slight bias in the Na^+ sorption data, which is mainly due to an overestimation of the population of Na^+ in the Stern layer sites, the model's performance is not significantly impaired. A bias in the population of the Stern layer species is not critical for the prediction of the sorption properties of strongly sorbing radioelements, such as transition metals, lanthanides or actinides. Surface complexes at the clay edge surfaces are the dominant sorbing species for these elements at trace conditions and overrule the contribution from Stern layer species. These surface complexes are not relevant with respect to surface diffusion because they are treated as immobile. Previous work (Glaus et al., 2015a, 2020) has demonstrated the model's applicability to a broad variety of cations with different chemical behaviours towards clay minerals and this work adds further support to the EDL model's capability to predict the diffusion behaviour of charges species in different sedimentary rocks.

The study demonstrates that accurately describing the diffusion and retardation properties of charged species in sedimentary rocks relies heavily on the chemical composition of the pore water. The clay rock samples used in the experiment were pre-equilibrated with synthetic pore waters that represent an average in situ pore water of the Opalinus Clay. However, it is important to note that this pore water composition may not be identical to the in situ conditions and that the ionic strength of the pore water can impact the effective diffusion coefficients (i.e. ratio of mobile surface species versus mobile aqueous species). The significance of ionic strength is evident in the spread between the model curves for $^{36}Cl^-$ and $^{22}Na^+$, which decreases with increasing ionic strength. The pore water composition of SPW-STA and SPW-TRU differ significantly in terms of the content of bivalent alkaline earth cations and sulfate and the monovalent Na^+ and Cl^-. Nonetheless, the calculated Donnan potential for these two pore waters is very similar, indicating that all types of charged solutes are important for the resulting enrichment or depletion factors between Donnan layer and bulk aqueous phase. The ionic strength appears to be an ideal indicator to for the description of the global effect of all cations and anions.

Declaration of competing interest

The authors declare that they have no known competing financial interests or personal relationships that could have appeared to influence the work reported in this paper.

Data availability

Data will be made available on request.

Acknowledgments

The authors would like to express their gratitude to several individuals and institutions who provided support for this study, including M. Mazurek, P. Wersin, T. Gimmi of the RWI (University of Bern), as well as D. Traber and J. Becker, and the technical illustration team, for sample selection, evaluation, auxiliary data and illustration support. Special thanks are extended to L. Van Laer and M. Aertsens (SCK CEN), C. Zwahlen and A. Jenni (RWI) for their valuable inputs and productive discussions. Finally, the authors acknowledge the financial support of the National Cooperative for the Disposal of Radioactive Waste (Nagra, Wettingen, Switzerland).

Abbreviations used in the context of the study areas and the locations of the drilling campaign (more details to be found in (Mazurek et al., 2023))

BOZ	Bözberg
BUL:	Bülach
MAR	Marthalen
STA	Stadel
TRU	Trüllikon
JO	Jura Ost
NL:	Nördlich Lägern
ZNO	Zürich Nordost

Appendix A. Supplementary data

Supplementary data to this article can be found online at https://doi.org/10.1016/j.apgeochem.2023.105842.

References

Altmann, S., Aertsens, M., Appelo, C.A.J., Bruggeman, C., Gaboreau, S., Glaus, M.A., Jacquier, P., Kupcik, T., Maes, N., Montoya, V., Rabung, T., Robinet, J.-C., Savoye, S., Schaefer, T., Tournassat, C., Van Laer, L., Van Loon, L.R., 2015. Processes of cation migration in clayrocks: Final scientific report of the Catclay European Project. Rapport CEA-R 6410, 140pp.

Appelo, C.A.J., Postma, D., 2005. In: Geochemistry, Groundwater and Pollution, second ed. A.A. Balkema Publishers, Leiden.

Appelo, C.A.J., Wersin, P., 2007. Multicomponent diffusion modeling in clay systems with application to the diffusion of tritium, iodide, and sodium in Opalinus Clay. Environ. Sci. Technol. 41, 5002–5007.

Appelo, C.A.J., Van Loon, L.R., Wersin, P., 2010. Multicomponent diffusion of a suite of tracers (HTO, Cl, Br, I, Na, Sr, Cs) in a single sample of Opalinus Clay. Geochim. Cosmochim. Acta 74, 1201–1219.

Aschwanden, L., Waber, H.N., Eichinger, F., Gimmi, T., 2024. Isotope diffusive exchange experiments for deriving porewater isotope composition in low-permeability rocks – Improvements in experimental procedure and data processing. Appl. Geochem. 160, 105844. https://doi.org/10.1016/j.apgeochem.2023.105844.

Baeyens, B., Bradbury, M.H., 2004. Cation exchange capacity measurements on illite using the sodium and cesium isotope dilution technique: effects of the index cation, electrolyte concentration and competition: modeling. Clays Clay Miner. 52, 421–431.

Chagneau, A., Tournassat, C., Steefel, C.I., Bourg, I.C., Gaboreau, S., Esteve, I., Kupcik, T., Claret, F., Schaefer, T., 2015. Complete restriction of Cl-36(-) diffusion by celestite precipitation in densely compacted illite. Environ. Sci. Technol. Lett. 2, 139–143.

Chen, Y., Glaus, M.A., Van Loon, L.R., Mäder, U., 2018. Transport of low molecular weight organic compounds in compacted illite and kaolinite. Chemosphere 198, 226–237.

Dufey, J.E., Laudelout, H.G., 1975. Self-diffusion of sodium on clay surfaces as influenced by two other alkali cations. J. Colloid Interface Sci. 52, 340–344.

Glaus, M.A., Aertsens, M., Appelo, C.A.J., Kupcik, T., Maes, N., Van Laer, L., Van Loon, L. R., 2015a. Cation diffusion in the electrical double layer enhances the mass transfer rates for Sr^{2+}, Co^{2+} and Zn^{2+} in compacted illite. Geochim. Cosmochim. Acta 165, 376–388.

Glaus, M.A., Aertsens, M., Maes, N., Van Laer, L., Van Loon, L.R., 2015b. Treatment of boundary conditions in through-diffusion: a case study of $^{85}Sr^{2+}$ diffusion in compacted illite. J. Contam. Hydrol. 177–178, 239–248.

Glaus, M.A., Baeyens, B., Bradbury, M.H., Jakob, A., Van Loon, L.R., Yaroshchuk, A., 2007. Diffusion of ^{22}Na and ^{85}Sr in montmorillonite: evidence of interlayer diffusion being the dominant pathway at high compaction. Environ. Sci. Technol. 41, 478–485.

Glaus, M.A., Birgersson, M., Karnland, O., Van Loon, L.R., 2013. Seeming steady-state uphill diffusion of $^{22}Na^{+}$ in compacted montmorillonite. Environ. Sci. Technol. 47, 11522–11527.

Glaus, M.A., Frick, S., Van Loon, L.R., 2020. A coherent approach for cation surface diffusion in clay minerals and cation sorption models: diffusion of Cs^{+} and Eu^{3+} in compacted illite as case examples. Geochim. Cosmochim. Acta 274, 79–96.

Glaus, M.A., Frick, S., Van Loon, L.R., 2021. Competitive effects of cations on the diffusion properties of strongly sorbing trace cations in compacted illite and Opalinus Clay. ACS Earth Space Chem. 5, 2621–2625.

Hummel, W., Thoenen, T., 2023. The PSI Chemical Thermodynamic Database 2020. Nagra Technical Report NTB 21-03. Nagra, Wettingen, Switzerland.

Jensen, D.J., Radke, C.J., 1988. Caesium and strontium diffusion through sodium montmorillonite at elevated temperature. J. Soil Sci. 39, 53–64.

Li, Y.H., Gregory, S., 1974. Diffusion of ions in sea water and in deep-sea sediments. Geochim. Cosmochim. Acta 38, 703–714.

Maes, N., Glaus, M.A., Baeyens, B., Marques Fernandes, M., Churakov, S.V., Dähn, R., Grangeon, S., Tournassat, C., Geckeis, H., Charlet, L., Brandt, F., Poonoosamy, J., Hoving, A., Havlova, V., Fischer, C., Scheinost, A.C., Noseck, U., Britz, S., Siitari-Kauppi, M., Missana, T., 2021. State-of-the-Art-report on the Understanding of Radionuclide Retention and Transport in Clay and Crystalline Rocks. Final Version as of 30.04.2021 of Deliverable D5.1 of the HORIZON 2020 Project EURAD. EC Grant agreement no, 847593.

Mazurek, M., Gimmi, T., Zwahlen, C., Aschwanden, L., Gaucher, E.C., Kiczka, M., Rufer, D., Wersin, P., Marques Fernandes, M., Glaus, M.A., Van Loon, L.R., Traber, D., Schnellmann, M., Vietor, T., 2023. Swiss deep drilling campaign 2019–2022: Geological overview and rock properties with focus on porosity and pore-space architecture. Appl. Geochem., 105839. https://doi.org/10.1016/j.apgeochem.2023.105839.

Molera, M., Eriksen, T., 2002. Diffusion of $^{22}Na^{+}$, $^{85}Sr^{2+}$, $^{134}Cs^{+}$ and $^{57}Co^{2+}$ in bentonite clay compacted to different densities: experiments and modeling. Radiochim. Acta 90, 753–760.

Nagra, 2014. SGT Etappe 2: Vorschlag weiter zu untersuchender geologischer Standortgebiete mit zugehörigen Standortarealen für die Oberflächenanlage: Charakteristische Dosisintervalle und Unterlagen zur Bewertung der Barrierensysteme. Nagra Technical Report NTB 14-03. Nagra, Wettingen, Switzerland.

Nagra, 2021. The Nagra Research, Development and Demonstration (RD&D) Plan for the Disposal of Radioactive Waste in Switzerland. Nagra Technical Report NTB 21-02. Nagra, Wettingen, Switzerland.

Shackelford, C.D., Daniel, D.E., 1991. Diffusion in saturated soil: I. Background. J. Geotech. Eng. ASCE 117, 467–484.

Stumm, W., Morgan, J.J., 1996. In: Aquatic Chemistry, third ed. J. Wiley & Sons.

Tinnacher, R.M., Holmboe, M., Tournassat, C., Bourg, I.C., Davis, J.A., 2016. Ion adsorption and diffusion in smectite: molecular, pore, and continuum scale views. Geochim. Cosmochim. Acta 177, 130–149.

Van Loon, L.R., Soler, J.M., Bradbury, M.H., 2003. Diffusion of HTO, $^{36}Cl^{-}$ and $^{125}I^{-}$ in Opalinus Clay samples from Mont Terri. Effect of confining pressure. J. Contam. Hydrol. 61, 73–83.

Van Loon, L.R., Soler, J.M., Müller, W., Bradbury, M.H., 2004. Anisotropic diffusion in layered argillaceous rocks: a case study with Opalinus Clay. Environ. Sci. Technol. 38, 5721–5728.

Van Loon, L.R., Jakob, A., 2005. Evidence for a second transport porosity for the diffusion of tritiated water (HTO) in a sedimentary rock (Opalinus Clay - OPA): application of through- and out-diffusion techniques. Transport Porous Media 61, 193–214.

Van Loon, L.R., Mibus, J., 2015. A modified version of Archie's law to estimate effective diffusion coefficients of radionuclides in argillaceous rocks and its application in safety analysis studies. Appl. Geochem. 59, 85–94.

Van Laer, L., Aertsens, M., Maes, N., Van Loon, L.R., Glaus, M.A., Wüst, R.A.J., 2024. Diffusion of HTO, ^{36}Cl and ^{22}Na in the Mesozoic rocks of northern Switzerland: III. Cross-lab comparison of diffusion measurements on argillaceous twin samples. Appl. Geochem. 160, 105840. https://doi.org/10.1016/j.apgeochem.2023.105840.

Van Loon, L.R., Bunic, P., Frick, S., Glaus, M.A., Wüst, R.A.J., 2023. Diffusion of HTO, ^{36}Cl and ^{22}Na in the Mesozoic rocks of northern Switzerland. I: Effective diffusion coefficients and capacity factors across the heterogeneous sediment sequence. Appl. Geochem. 159, 105843. https://doi.org/10.1016/j.apgeochem.2023.105843.

van Schaik, J.C., Kemper, W.D., Olsen, S.R., 1966. Contribution of adsorbed cations to diffusion in clay-water systems. Soil Sci. Soc. Am. Proc. 30, 17–22.

Wersin, P., Gimmi, T., Ma, J., Mazurek, M., Zwahlen, C., Aschwanden, L., Gaucher, E.C., Traber, D., 2023. Porewater profiles of Cl and Br in boreholes penetrating the Mesozoic sequence in northern Switzerland. Appl. Geochem. 159, 105845. https://doi.org/10.1016/j.apgeochem.2023.105845.

Wigger, C., Kennell-Morrison, L., Jensen, M., Glaus, M.A., Van Loon, L.R., 2018. A comparative anion diffusion study on different argillaceous, low permeability sedimentary rocks with various pore waters. Appl. Geochem. 92, 157–165.

Zwahlen, C., Gimmi, T., Jenni, A., Kiczka, M., Mazurek, M., Van Loon, L.R., Mäder, U., Traber, D., 2024. Chloride accessible porosity fractions across the Jurassic sedimentary rocks of northern Switzerland. Applied Geochem., 105841. https://doi.org/10.1016/j.apgeochem.2023.105841.